J|A|C|S
ARTICLES
Published on Web 12/21/2002

A New Model for Simulating 3-D Crystal Growth and Its Application to the Study of Antifreeze Proteins

Brent Wathen,[†] Michael Kuiper,[‡] Virginia Walker,[‡] and Zongchao Jia*,[†]

Contribution from the Departments of Biochemistry and Biology, Queen's University, Kingston, Ontario, Canada K7L 3N6

Received May 4, 2002; E-mail: jia@post.queensu.ca

Abstract: A novel computational technique for modeling crystal formation has been developed that combines three-dimensional (3-D) molecular representation and detailed energetics calculations of molecular mechanics techniques with the less-sophisticated probabilistic approach used by statistical techniques to study systems containing millions of molecules undergoing billions of interactions. Because our model incorporates both the structure of and the interaction energies between participating molecules, it enables the 3-D shape and surface properties of these molecules to directly affect crystal formation. This increase in model complexity has been achieved while simultaneously increasing the number of molecules in simulations by several orders of magnitude over previous statistical models. We have applied this technique to study the inhibitory effects of antifreeze proteins (AFPs) on ice-crystal formation. Modeling involving both fish and insect AFPs has produced results consistent with experimental observations, including the replication of ice-etching patterns, ice-growth inhibition, and specific AFP-induced ice morphologies. Our work suggests that the degree of AFP activity results more from AFP ice-binding *orientation* than from AFP ice-binding *strength*. This technique could readily be adapted to study other crystal and crystal inhibitor systems, or to study other noncrystal systems that exhibit regularity in the structuring of their component molecules, such as those associated with the new nanotechnologies.

Introduction

Computational techniques for modeling chemical and biochemical processes have progressed in recent years as a result of advances in both computing power and software engineering. Limits to existing computing power, however, continue to divide computational studies of molecular interactions into two categories: those that attempt mathematical treatments of the atomic forces within and between molecules but as a consequence consider only a small number of molecules, and those that forego these mathematical treatments to model vastly larger systems of molecules through the use of simplified molecular representations and statistical descriptions of molecular interactions. Techniques in the former category, such as molecular dynamics and energy minimization, typically aim at understanding the specific nature of chemical processes such as protein−ligand interactions, whereas techniques in the latter category are useful for studying molecular cooperation or competition in large systems.

Although it is not currently feasible to incorporate detailed molecular mechanics calculations into systems containing millions of molecules (consider, for example, a recent computationally demanding study of ice formation that included 512 water molecules at the freezing point[1]), some areas of research would benefit from a better mixture of these two computational approaches. One such area is the study of antifreeze proteins (AFPs) and their interactions with ice. AFPs are structurally diverse proteins that contribute to the survival of many organisms living in cold environments. In vitro experiments have demonstrated that ice-crystal growth in the presence of AFPs can be inhibited over a range of supercooled temperatures that is dependent on the particular AFP in solution and its concentration.[2] This growth inhibition is accompanied by specific AFP-dependent changes to ice-crystal morphology.[3] AFPs are thought to inhibit ice growth by adsorbing to ice surfaces,[4] restricting subsequent ice growth to curved surfaces between bound AFPs.[5] This additional curvature increases the local surface-area-to-volume ratio of the ice front, retarding ice growth due to the unfavorable thermodynamic free energy change associated in creating the extra surface area. The degree of surface curvature exhibited is temperature dependent, with lower temperatures stabilizing steeper curvatures; as temperature decreases, a critical point is reached where AFPs can no longer inhibit ice growth, and a rapid burst of crystal formation ensues. Unfortunately, gathering experimental evidence for this theory has proven difficult, primarily because the fragile nature of AFP ice-crystal structures does not lend itself to X-ray crystallographic and NMR studies. Consequently, although ice-surface recognition

* To whom correspondence should be addressed. Tel: 613 533 6277. Fax: 613 533 2497.
[†] Department of Biochemistry.
[‡] Department of Biology.

(1) Matsumoto, M.; Saito, S.; Ohmine, I. *Nature* **2002**, *416*, 409−413.
(2) Davies, P. L.; Hew, C. L. *FASEB J.* **1990**, *4*, 2460−2468.
(3) Hew, C. L.; Yang, D. S. C. *Eur. J. Biochem.* **1992**, *203*, 33−42.
(4) Madura, J. D.; Baran, K.; Wierzbicki, A. *J. Mol. Recognit.* **2000**, *13*, 101−113.
(5) Raymond, J. A.; DeVries, A. L. *Proc. Natl. Acad. Sci. U.S.A.* **1977**, *74*, 2589−2593.

10.1021/ja0267932 CCC: $25.00

is undoubtedly crucial for AFP activity, it is unknown just how a particular stereospecific AFP−ice interaction influences AFP activity and why, for instance, some insect AFPs have 10−100 times more antifreeze activity on a molar basis than fish AFPs. The lack of experimental evidence has spawned numerous molecular dynamics studies of AFP−ice interactions, most of which focus on measuring the "binding energy" between AFPs and predetermined ice slabs, either with or without accompanying aqueous water molecules.[4,6−11] While these experiments, together with numerous biochemical experiments,[12−16] have generated much debate as to AFP ice-binding orientations and the forces involved in AFP−ice interactions, they have not been able to address fundamental mechanistic questions, both because of their limited scope (generally involving one or at most several AFPs interacting with an ice block containing upward of 10 000 water molecules) and because of their treatment of ice blocks as static objects that neither grow nor melt. Obviously, there is need for a modeling technique based on statistical models that incorporates structural and electrostatic properties of participating molecules, allowing specific molecular shapes and surface charge distributions to influence statistical crystal growth.

To address this fundamental gap between the two basic approaches to molecular modeling, and to aid us in the investigation of AFP ice-growth inhibition, we have developed a new computational technique that combines the use of detailed 3-D molecular shapes together with precalculated energetics information into a statistical model that is ideally suited for the study of crystal systems containing large numbers of interacting molecules. We report this model herein, together with the initial application of this model to the study of AFP−ice interactions.

General Modeling Technique

Our model is based on an extension to the Kinetic Ising model as described by Gilmer.[17] It simulates the dynamic formation of regular crystal structures composed from a collection of 3-D molecules with arbitrary shape. Central to the model is the concept of the *simulation space*, which is a regular arrangement of spatial locations and inherent connections that governs the possible placements of molecules in the simulation and dictates what neighboring interactions can occur. The nature of this arrangement is problem dependent, but should be chosen so as to reflect the actual arrangement and interactions of the elementary molecules in the crystal being modeled. It must be stressed that only molecules that are in the solid state and that are bound to a crystal structure are represented in simulations; molecules in the liquid or gaseous state are not represented in simulations until they undergo a phase transition to the solid state and join a growing crystal. Furthermore, all molecules in simulations are spatially restricted to a single orientation with respect to the underlying regular arrangement of simulation space locations, although symmetric transformations about an origin are permitted to allow molecules to interact with all faces of a crystal. With this restriction, all molecules within simulations can then be defined spatially by specific 3-D collections of relative simulation space locations. As in the Ising model,[17] simulation space locations are either occupied or unoccupied, only one molecule can occupy a location at a time, and interactive forces only occur between neighboring locations as defined by the inherent connectivity of the simulation space.

The challenge of simulating the growth of true 3-D structures containing thousands or millions of molecules was met by the selection of efficient data storage mechanisms and fast algorithms. To balance the requirements of mass storage and rapid access, the occupied simulation space locations were logically separated into *surface* locations (those occupied locations that have at least one unoccupied neighboring location) and *buried* locations (those occupied locations that have all of their neighbors likewise occupied) (Figure 1). For large simulation spaces, the vast majority of the occupied locations are buried, and so do not participate in the simulation other than to define the structure morphology. Simulation spaces are therefore stored in a semicompressed array, wherein the surface locations are left uncompressed to be readily available, while buried locations are stored in a compressed format, allowing for much larger simulation spaces than would otherwise be possible. Furthermore, true 3-D simulation is achieved by maintaining separate lists of *interface* locations, where these are defined either as occupied, nonburied locations or as unoccupied locations next to occupied locations (Figure 1). All crystal association and dissociation events necessarily occur at these interface locations. These lists allow for the rapid selection of any 3-D position on the surface of a structure to which a molecule can either join or detach.

To incorporate energetics information into a statistical model, the spatial freedom of participating molecules is restricted to a single 3-D orientation with respect to the underlying arrangement of simulation space locations. This implies that for each type of simulation molecule, the set of simulation space locations that represent its volume, both in the trivial instance of a single location (as in the case for water molecules in our AFP-ice models discussed below) as well as in the more complex case of multiple locations (such as for the larger AFP molecules in these same models), can be determined *a priori*. This restriction ensures that pairs of molecules in simulations only interact in a *finite number of predeterminable orientations*. The energy of interaction between each of these finite pairings can then be calculated using the more detailed computational techniques of molecular dynamics and energy minimization *prior* to the introduction of these molecules into simulations (Figure 1B).

Dynamic crystal growth during simulations results from the competition between two classes of random events that occur at interface locations on crystal surfaces, association events that cause a molecule to join a crystal and dissociation events that cause a molecule to detach from a crystal. Events are selected

(6) Madura, J. D.; Wierzbicki, A.; Harrington, J. P.; Maughon, R. H.; Raymond, J. A.; Sikes, C. S. *J. Am. Chem. Soc.* **1994**, *116*, 417−418.
(7) Wierzbicki, A.; Taylor, M. S.; Knight, C. A.; Madura, J. D.; Harrington, J. P.; Sikes, C. S. *Biophys. J.* **1996**, *71*, 8−18.
(8) Yang, D. S. C.; Hon, W. C.; Bubanko, S.; Xue, Y.; Seetharaman, J.; Hew, C. L.; Sicheri, F. *Biophys. J.* **1998**, *74*, 2142−2151.
(9) McDonald, S. M.; White, A.; Clancy, P.; Brady, J. W. *AIChE J.* **1995**, *41*, 959−973.
(10) Dalal, P.; Knickelbein, J.; Haymet, A. D. J.; Sönnichsen, F. D.; Madura, J. D. *Phys. Chem. Commun.* **2001**, *7*, 1−5.
(11) Hayward, J. A.; Haymet, A. D. *J. Chem. Phys.* **2001**, *114*, 3713−3726.
(12) Yang, D. S. C.; Sax, M.; Chakrabartty, A.; Hew, C. L. *Nature* **1988**, *333*, 232−237.
(13) Chao, H.; Houston, M. E., Jr.; Hodges, R. S.; Kay, C. M.; Sykes, B. D.; Loewen, M. C.; Davies, P. L.; Sonnichsen, F. D. *Biochemistry* **1997**, *36*, 14652−60.
(14) Haymet, A. D.; Ward, L. D.; Harding, M. M.; Knight, C. A. *FEBS Lett.* **1998**, *430*, 301−306.
(15) Baardsnes, J.; Kondejewski, L. H.; Hodges, R. S.; Chao, H.; Kay, C.; Davies, P. L. *FEBS Lett.* **1999**, *463*, 87−91.
(16) Jia, Z.; DeLuca, C. I.; Chao, H.; Davies, P. L. *Nature* **1996**, *385*, 285−288.
(17) Gilmer, G. H. *Science* **1980**, *208*, 355−363.

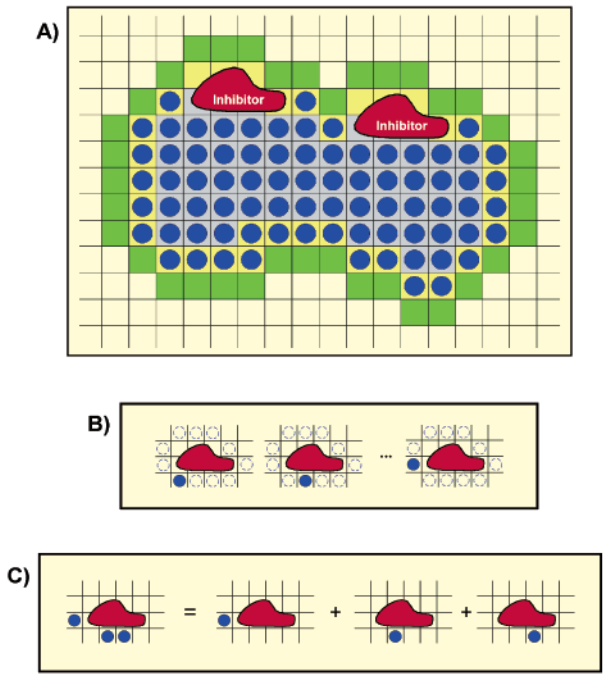

Figure 1. Simulation concepts are presented here in two dimensions for clarity. Panel A shows a snapshot of a simulation space partially occupied by blue crystal molecules and red "inhibitor" molecules (occupying seven simulation space locations each). Gray boxes indicate *buried* locations, yellow boxes represent *surface* locations, and yellow and green boxes together comprise *interface* locations. Association events occur at green interface locations, while dissociation events occur at yellow interface locations. The method for predetermining energetics information is shown in panel B. All neighboring orientations between a crystal molecule and an inhibitor are determined (shown for illustrative purposes by dashed circles). The interaction energy between the inhibitor and each of the neighboring crystal molecules is precalculated using an energetics technique such as molecular dynamics or energy minimization. Three of the predeterminable orientations are shown. This precalculated energetics information is then used to determine interaction energies during simulations, as shown in panel C. The interaction energy between the inhibitor molecule and its neighboring crystal molecules in the configuration shown in the left portion of this panel would be determined by summing the precalculated interaction energies between the inhibitor and each of the occupied neighboring positions, as indicated.

at random on the basis of the defined probability functions that use the precalculated interaction energies when considering the likelihood of association/dissociation events at interface locations. Following an association or a dissociation event, both the simulation space and the interface lists are updated, and the process is repeated.

The Model Applied: AFP Ice-Growth Simulations

Our computational model was applied to the study of AFPs and their effects on ice-crystal growth. Regular hexagonal ice, ice I_h, is a crystal belonging to the $P6_3/mmc$ space group where each internal water molecule makes four tetrahedrally arranged hydrogen bonds to neighboring water molecules.[18] As can be seen in Figure 2, the arrangement of water molecules and the resulting hydrogen-bond network in ice I_h produce ice crystals with distinctive orientations that can be described using a set of internal *a*- and *c*-axes. Using these axes, it is possible to describe specific planes of ice, either in terms of these axes directly (for example, the *basal plane*, which is perpendicular

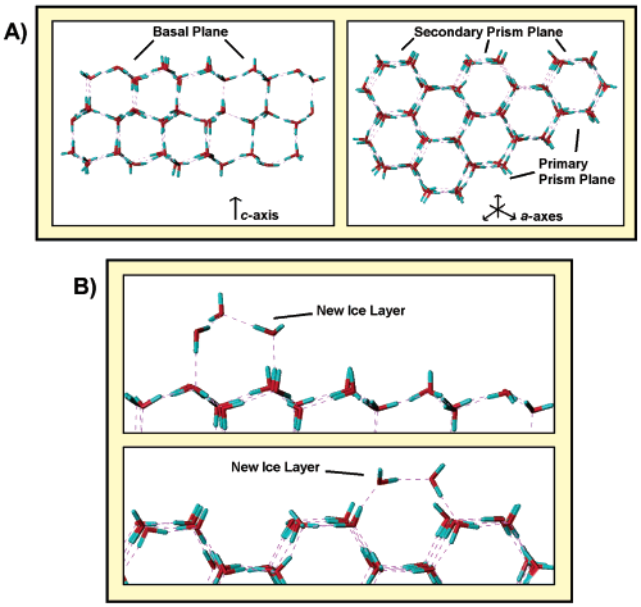

Figure 2. Ice I_h structure. Panel A shows two views of the water molecule alignment within ice I_h and the resulting hydrogen-bonding network (purple). The left view is looking down the secondary prism plane, with the basal plane on the top. The right view is a 90° rotation of the left view bringing the basal plane face on, showing the relationship between the primary, secondary, and prism planes. The internal ice axes are as indicated. Panel B shows the alignment of aqueous water molecules required to produce nucleation events on the basal, primary prism, and secondary prism planes. Notice the orientation of the hydrogen-bond network. This orientation influences growth rates out of the various ice planes.

to the *c*-axis, or the *secondary prism plane*, which is perpendicular to the *a*-axis) or, for pyramidal planes that are not at convenient angles to the *a*- and *c*-axes, indirectly in terms of Miller−Bravis indices.[19] In general, regular ice growth proceeds along a plane in a two-step process: first, a nucleation event occurs perpendicular to the plane, creating a new layer of ice; this is then followed by rapid growth parallel to the plane as this new layer expands.[20] However, ice growth is not uniform in all directions. This phenomenon, termed anisotropic growth, results from differences in the orientation of the hydrogen-bond network along different planes of ice, in effect making it spatially more difficult to stabilize new growth in the basal plane direction than in either the primary or the secondary prism plane directions (Figure 2). Indeed, ice crystals grown at low degrees of supercooling are known to grow as flat, circular disks,[21] reflecting the fact that growth in the basal direction is almost negligible (producing the flat surfaces of the crystals), while growth in the primary and secondary prism directions is roughly equal (producing the circular morphology of the crystals).

To correctly model the anisotopic growth nature of ice, a simulation space with an arrangement of spatial locations that matched the oxygen atom arrangement within hexagonal ice I_h crystals was adopted (Figure 2). Each location in the simulation space was separated by 2.76 Å in a tetrahedral arrangement from its four neighboring locations, ensuring that the ice I_h hydrogen-bond network was incorporated into the model. Using this arrangement, each water molecule in an ice crystal, hereafter

(18) Hobbs, P. V. *Ice Physics*; Oxford University Press: New York, 1974; p 18.

(19) Hobbs, P. V. *Ice Physics*; Oxford University Press: New York, 1974; p 725.

(20) Hobbs, P. V. *Ice Physics*; Oxford University Press: New York, 1974; p 556.

(21) Maruyama, M.; Ashida, T.; Knight, C. A. *J. Cryst. Growth* **1999**, *205*, 391−394.

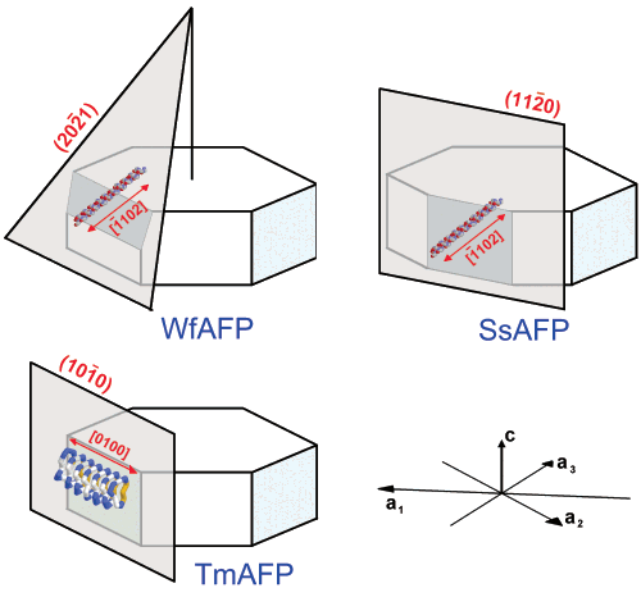

Figure 3. Ice adsorption planes and ice alignment of three AFPs. The alignments of two fish AFPs, isoform Hplc6 of winter flounder AFP (WfAFP) and isoform ss8 of shorthorn sculpin AFP (SsAFP), and of a beetle AFP from *tenebrio molitor* (TmAFP) are shown and labeled using Miller−Bravis indices. Ice axes are indicated in the bottom right corner for reference.

referred to as an ice molecule, occupies a single simulation space location. Two fish Type I AFPs, from shorthorn sculpin (SsAFP) and winter flounder (WfAFP), and an insect AFP from *Tenebrio molitor* (TmAFP), were selected for inclusion in simulation experiments. Figure 3 describes the experimentally derived docking orientations of these three AFPs that have arisen from structure determination[12,22] and ice-etching studies.[7,23] Molecular dynamics and energy minimization techniques (performed with the SYBYL software package[24] using the Tripos force field with Gasteiger/Marsili charges) were used to generate AFP-ice docking models consistent with the orientations described in Figure 3. Each docking model then served as a template for creating a representation of an AFP for use in simulations, which consisted of a listing of all relative simulation space locations that describe the volume occupied by each oriented AFP. SYBYL was used to precalculate the interaction energy between each possible neighboring orientation of an ice molecule and an AFP molecule (as in Figure 1B).

Because we were primarily concerned with AFP effects on ice-crystal formation, all AFP-ice simulations were *crystal-centric*; that is, interactions that did not involve the ice crystal were ignored. All molecular association and dissociation events, therefore, were with respect to an ice crystal. Any molecule that did not have a neighboring ice molecule in simulation was automatically removed from the simulation. Furthermore, any AFP−AFP interactions were ignored.

The probability of a water molecule either joining or detaching from an ice crystal was dependent upon the number of hydrogen bonds being formed or broken during the association/dissociation event. Because these events necessarily occur at interface locations, they involve the forming or breaking of up to three hydrogen bonds. These association/dissociation probabilities, referred to as the water *on* rates, k_i^+, and water *off* rates, k_i^-, where i bonds are formed or broken, are temperature dependent, and were derived from the relationship between equilibrium ice-crystal size and temperature as follows. It can be shown[25] that the temperature-dependent critical radius r of an ice embryo, below which the crystal will spontaneously melt, and above which the crystal will spontaneously grow, is

$$r = (2\sigma_{LS})/n_S kT \ln(p_L/p_S) \quad (1)$$

where σ_{LS} is the interfacial free energy between the water and ice, n_S is the number of molecules per unit volume of ice, T is temperature, k is Boltzmann's constant, and p_L and p_S represent the vapor pressures over water and ice, respectively. A relationship between water *on/off* probabilities and temperature was established by determining sets of these *on/off* probabilities that maintained crystals of varying sizes at equilibrium, and then by relating the radii of these equilibrated crystals to temperatures using eq 1. Because ice crystals at low degrees of supercooling are known to adopt circular disk morphologies,[21] we created a set of 38 crystals with this morphology (done by collecting intermediary crystals, ranging in radius from 82.7 to 526.5 Å with proportionate differences in disk thickness, from a simulation designed to induce circular disk morphological growth from an initial seed crystal) and sought sets of on/off probabilities that would maintain both the morphology and the volume of these crystals. At equilibrium conditions, the number of water molecules joining and leaving an ice crystal are equal, so that

$$k_1^- ice_1 + k_2^- ice_2 + k_3^- ice_3 = k_1^+ water_1 + k_2^+ water_2 + k_3^+ water_3 \quad (2)$$

where ice_i and $water_i$ signify the total numbers of occupied surface locations and unoccupied locations adjacent to the surface, respectively, with i occupied neighbors. Approximations for the ice_i and $water_i$ values as functions of radius r were determined by extrapolating from actual counts of these values from the 38 chosen ice crystals:

$$ice_1(r) = 0.0669r^2 - 0.8198r \quad (3)$$

$$ice_2(r) = 0.2686r^2 - 2.6351r \quad (4)$$

$$ice_3(r) = 0.7737r^2 - 14.334r \quad (5)$$

$$water_1(r) = 0.7741r^2 - 9.2009r \quad (6)$$

$$water_2(r) = 0.2600r^2 - 3.5812r \quad (7)$$

$$water_3(r) = 0.0725r^2 - 1.9011r \quad (8)$$

As with other crystal growth simulations,[17] the assumption that crystal growth proceeds from the melt without significant surface diffusion was adopted. Because this implied that the water *on* rate is independent of position, it allowed for the use of a single k^+ *on* rate in place of the multiple k_i^+ values. The remaining unknowns in eq 2, k^+ and k_i^-, form a relative set; therefore, k^+ was set arbitrarily. As a further simplification, the relationship between k_2^- and k^+ under equilibrium conditions, given by

(22) Liou, Y. C.; Tocilj, A.; Davies, P. L.; Jia, Z. *Nature* **2000**, *406*, 322−4.
(23) Knight, C. A.; Cheng, C. C.; DeVries, A. L. *Biophys. J.* **1991**, *59*, 409−418.
(24) Tripos Associates, St. Louis, Missouri.

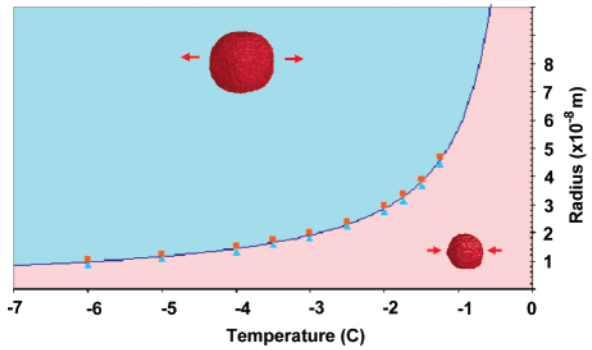

Figure 4. Ice-only simulations along the growth-melt boundary. The graph of eq 1, relating equilibrium temperature to ice-crystal radius, is shown in blue. Positions above this line should spontaneously grow, while those below this line should spontaneously melt. Results from a series of ice-only simulations undertaken to verify water *on/off* rates are indicated in the figure. The symbol locations on the graph indicate the radii of initial ice crystals used, together with selected simulation temperatures. Red squares indicate crystals that underwent spontaneous growth, both in disk radius and in disk thickness; blue triangles indicate crystals that spontaneously melted in both of these dimensions.

Gilmer and Bennema,[27] was adopted:

$$k_2^- = (p_L/p_S)k^+ \tag{9}$$

where p_L and p_S are the temperature-dependent saturated partial pressures over water and ice, respectively. Equations relating p_L and p_S to temperature (T) were derived by extrapolation from physical data:[28]

$$p_L = 4.6007\mathrm{e}^{0.0756T} \tag{10}$$

$$p_S = 4.6001\mathrm{e}^{0.083T} \tag{11}$$

Finally, through repeated simulations, values for k_1^- were individually discovered for all 38 crystals that maintained these crystals at equilibrium (as determined by total number of water molecules, size of crystals in the X, Y, and Z directions, and visual inspection of the resulting crystal morphology). Extrapolation from the resulting k_1^- values gives the following relationship between k_1^- and temperature (T):

$$k_1^- = -3.0 \times 10^{-4}T \tag{12}$$

Substituting eqs 3−12 into eq 2, and using eq 1 to relate radius to temperature, allowed us to solve for the remaining variable k_3^- as a function of temperature. As can be seen in Figure 4, verification of the temperature-dependent water probability functions through independent melt/growth simulations with crystals of varying sizes and at various temperatures suggests that these functions provide an accurate representation of temperature within simulations.

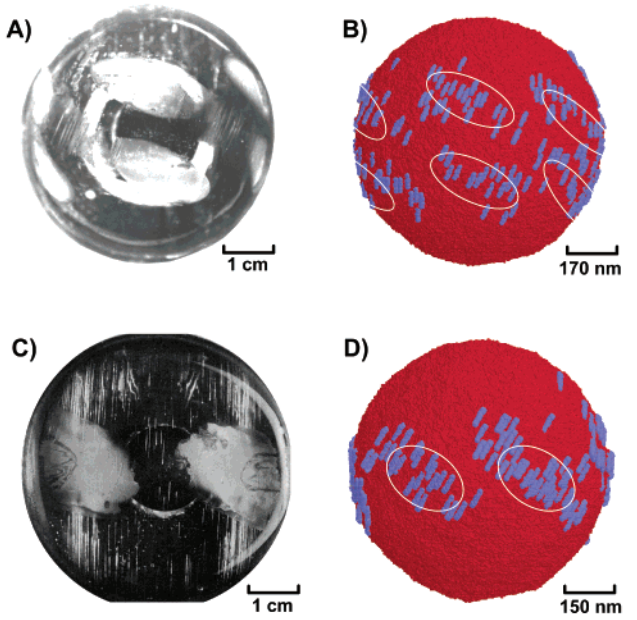

Figure 5. Comparison of AFP ice-etching simulations with actual AFP ice-etching experiments, using WfAFP (A and B) and SsAFP (C and D). Both AFPs bind with the same relative alignment to ice (see Figure 2) but to different ice planes, resulting in distinctive ice-etching patterns. As in ice-etching experiments developed by Knight et al.,[16] we transferred ice hemispheres to dilute solutions of AFPs (~<0.01 mg/mL) to deduce preferential ice-binding planes, which appear as etched or frosted regions on hemispheres A and C. In our simulations, low AFP concentration was simulated by lowering AFP *on* rates to develop similar ice-binding patterns although on vastly different scales. The modeled AFPs (appearing as blue cylinders) are adsorbed over the ice lattice surface (large red spheres) in B and D. White ovals have been added to the simulated surfaces to highlight adsorption planes. (Part C was adapted from ref 7.)

The selection of probability functions to govern AFP association/dissociation events was more experimental. In general, though, on the basis of the assumption that the rate of AFP associations is determined primarily by the AFP diffusion rate in the melt, a single AFP *on* rate, $kAFP^+$, was used. Various series of AFP *off* rates, $kAFP^-$, were tested; all were dependent on the current interaction energy between an AFP and the ice crystal. This interaction energy was a summation of the individual precalculated interaction energies between an AFP and each of the neighboring simulation space locations *that were currently occupied by ice molecules* (as in Figure 1C). All series of AFP *off* rates that were tested contained an inverse relationship between interaction energy and dissociation rate, reflecting the fact that AFPs with a snug fit to ice have a lower probability of disassociating than do loosely fit AFPs.

The AFP binding specificity of our model was tested with simulations using two different Type I AFPs, WfAFP and SsAFP. These AFPs have similar docking orientations to ice, although to different ice planes (Figure 3). Each of these AFPs was incorporated into simulations involving large spherical crystals (containing 10 million water molecules) that provided all possible surfaces for potential AFP adsorption. Figure 5 shows the results of these simulations after 100 million association/dissociation events involving both water and AFP molecules, at conditions selected to induce minimal or no ice growth. As can be seen, the AFPs accumulated at ice positions that were consistent with their stereospecificity. Although many

(25) Turnbull and Fisher[26] reasoned that the free energy change ΔGLS associated with the creation of a spherical ice crystal of radius r from supercooled liquid (assuming the crystal is isotropic for ease of calculation) is $\Delta GLS = nS(\mu S - \mu L)(4/3\pi r^3) + \sigma LS(4\pi r^2)$ (eq 13), where μS and μL are the chemical potential per water molecule in ice and supercooled water respectively, nS is the number of molecules per unit volume of ice, and σLS is the interfacial free energy between the water and ice. The $(\mu S - \mu L)$ term can be approximated by $-kT\ln(pL/pS)$, where pL and pS represent the vapor pressures over water and ice, respectively, at temperature T and using Boltzmann's constant k. Substituting into eq 13 and setting $\partial\Delta GLS/\partial r = 0$ gives the temperature-dependent critical size of an ice embryo expressed in eq 1.

(26) Turnbull, D.; Fisher, J. C. *J. Chem. Phys.* **1949**, *17*, 71.
(27) Gilmer, G. H.; Bennema, P. *J. Cryst. Growth* **1972**, *13/14*, 148−153.
(28) *CRC Handbook of Chemistry and Physics*, 61st ed.; CRC Press: Boca Raton, FL, 1981.

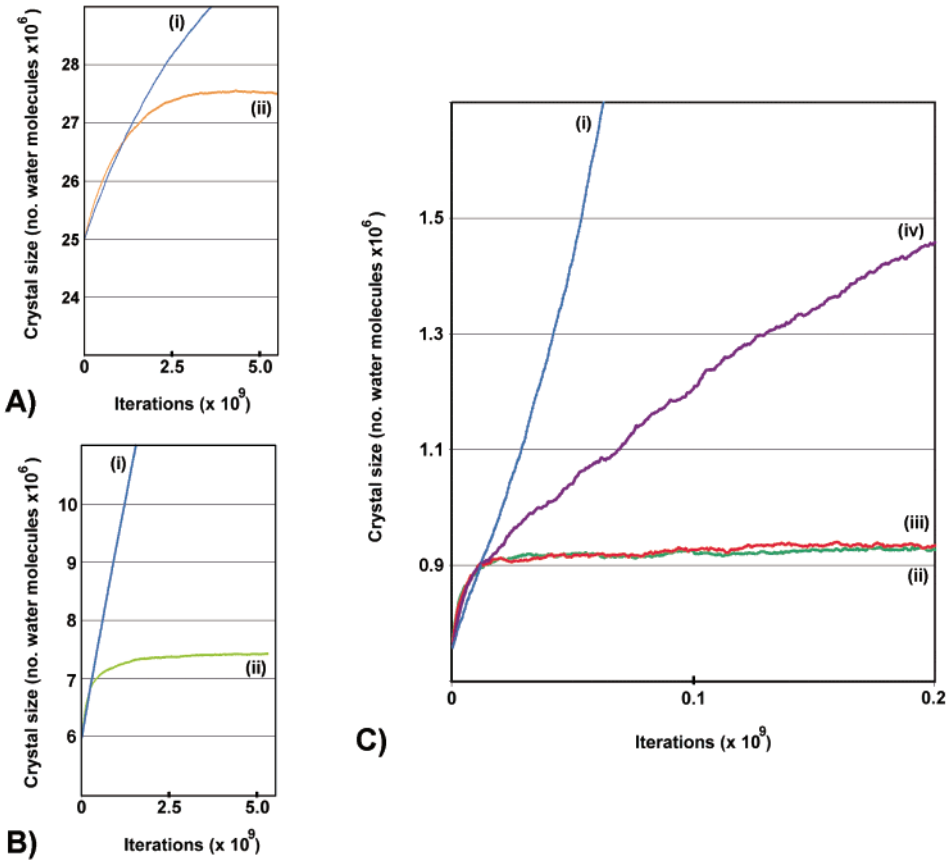

Figure 6. The effects of AFPs on ice growth in simulation. Graph A shows the growth rates of a 25 million water molecule ice crystal grown at a simulation temperature of −2 °C over prolonged simulation time, both without AFPs (line i) and in the presence of WfAFP (line ii). Similarly, graph B shows the growth of a 6 million water molecule ice crystal grown at a simulation temperature of −4.5 °C, both without AFP (line i) and in the presence of TmAFP (line ii). In both cases, ice growth is inhibited over prolonged simulation times by the presence of AFPs. Graph C compares the antifreeze abilities of WfAFP and TmAFP directly. Here, an initial seed crystal containing 750 000 water molecules is grown under varying AFP conditions −3.5 °C. Line i shows unrestricted ice growth without AFPs. Line ii shows ice-growth inhibition in the presence of TmAFP, as does line iii but using a doubled AFP *off* rate (which effectively halves the relative AFP binding strength). Increasing the TmAFP *off* rate had little effect on its antifreeze ability. In contrast, line iv shows ice growth in the presence of WfAFP despite using an *off* rate *reduced* from (ii) by 80% (effectively increasing by 5-fold its binding strength).

orders of magnitude smaller than the results of actual ice-etching studies involving these same proteins,[7,23] the binding patterns exhibited in both simulation experiments and ice-etching studies show a clear resemblance. Altering AFP *off* rates for both of these AFPs did not significantly change the pattern of distribution on the ice surface, although higher AFP *off* rates, mimicking weaker binding, did result in a less dense pattern. As one would expect, it appears as if AFPs were more likely to remain bound if most of their ice-binding surface was in direct contact with the ice, a condition that was best satisfied when they adsorbed close to their optimum binding locations.

Longer simulations using a fish Type I AFP (WfAFP) and an insect AFP (TmAFP) were performed to investigate the antifreeze abilities of AFPs in simulations. These simulations began with larger initial crystals and were run at simulation temperatures approximating the reported maximal freezing point depression for these AFPs[29] (25 million initial water molecules at −2.0 °C for WfAFP; 8 million initial water molecules at −4.5 °C for TmAFP). As can be seen in Figure 6A and B, both AFPs were able to achieve ice-growth inhibition over extended simulation time (more than 5 billion association/dissociation events). To directly compare their antifreeze abilities, simulations using the same initial crystal size (containing 750 000 water molecules) and constant temperature (−3.5 °C) were run with each of these AFPs (Figure 6C). TmAFP was able to inhibit ice growth under these conditions, while WfAFP was not. Furthermore, artificially increasing the TmAFP *off* rates by a factor of 2 (weakening AFP-ice binding) did not greatly reduce its ice-inhibition effectiveness, while artificially decreasing the WfAFP *off* rates by a factor of 5 (strengthening AFP-ice binding) did not significantly improve the effectiveness of this AFP. Lower binding strength, however, did eventually reach a point where ice inhibition activity is totally abolished. Indeed, in the case of TmAFP, it was not until the AFP *off* rates were substantially increased ($> \times 10$) that all activity appeared to be lost and the ice crystals grew continuously.

Prolonged simulations using WfAFP and TmAFP also produced morphologies similar to those observed experimentally[3,22] (Figure 7A,B,E,F). Ice crystals grown in simulations with WfAFP show clear bipyramidal growth, while those grown in simulations with TmAFP produce lemon-shaped, biconcave crystals. Furthermore, simulations run at temperatures below the antifreeze abilities of both WfAFP and TmAFP produce burst growth in patterns that mimic experimentally observed burst growth phenomena[3,22] (Figure 7C,D,G,H). In the case of WfAFP, simulations at reduced temperatures produced the

(29) Graham, L. A.; Liou, Y. C.; Walker, V. K.; Davies, P. L. *Nature* **1997**, *388*, 727−728.

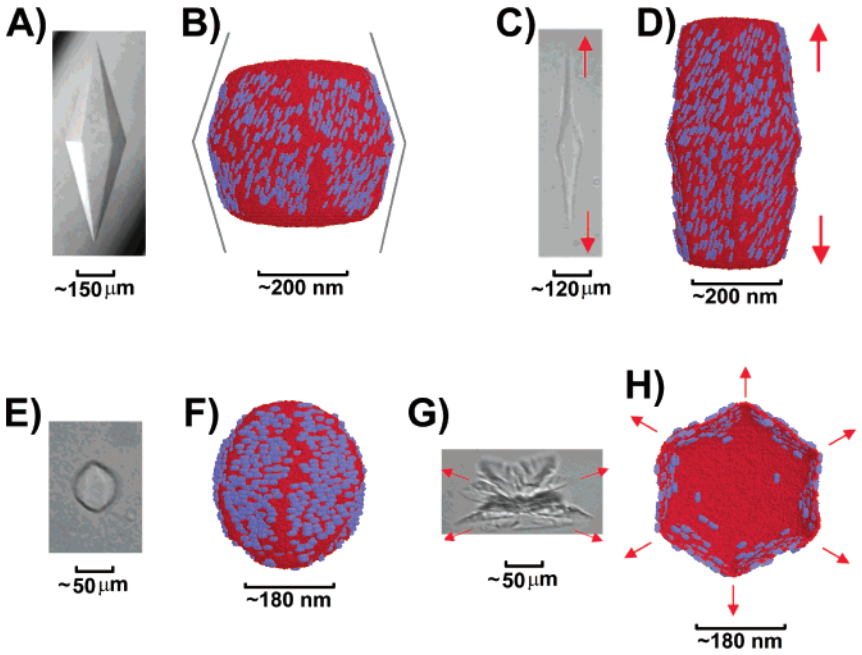

Figure 7. Comparison of experimental ice morphologies with simulation ice morphologies. Ice-crystal studies were performed using a nanoliter osmometer (Clifton Technical Physics, Hartford, NY). (A) shows a stable hexagonal bipyramid crystal grown in the presence of WfAFP. (B) shows the morphological effects of WfAFP on ice growth in simulation, with lines added to highlight inhibited ice planes. (C) shows burst morphology of ice in the presence of WfAFP, with distinctive spicular growth along the *c*-axis, as indicated by the arrows. The simulated burst morphology also shows spicular growth in (D). (E) illustrates biconcave morphology of ice crystals grown in the presence of TmAFP. (F) shows similar biconcave morphology observed in ice simulations using TmAFP. The crystal in (E) undergoes rapid burst growth in the direction of the arrows, as shown in (G). (H) is the burst simulation of (F) (looking down the *c*-axis). Notice the highly unusual concave morphology during burst growth, caused by the increasing curvature between bound TmAFP molecules that appears as temperatures are lowered. Note that the simulated crystals are on a vastly smaller scale than the experimental crystals. For example, the sharp apex in (A) appears as a rounded surface in (B) due to the highly magnified scale.

distinctive, *c*-axis aligned, spicular morphology as ice grew out of the wholly exposed basal planes. With TmAFP, burst growth during simulations at reduced temperatures was aligned perpendicular to the *c*-axis out of the secondary prism plane, producing highly unusual concave ice surface growth (Figure 7H).

Figure 8, showing close-up views of prism plane growth both in the absence and in the presence of AFPs, provides visual support for the prevailing theories concerning the mechanisms of both ice growth[20] and AFP ice-growth inhibition.[4,5] In Figure 8A, step growth is clearly evident, as newly nucleated layers of the prism plane are seen to be growing out toward the edges of the plane. The regularity of unmediated ice growth in this figure is in stark contrast to the AFP-induced bulging growth seen in Figure 8B, where bound AFPs dramatically increase the local curvature of ice growing in their proximity.

Discussion

We have developed a new computational technique for investigating regular crystal structures that advances current statistical crystal-formation models in several critical areas. These include an extension of the current 3-D surface modeling to true 3-D volume modeling, an increase in the number of molecules involved in simulations by several orders of magnitude, and an incorporation of both 3-D spatial geometry and precalculated interaction energies into simulations. Because these latter energies can be calculated using techniques such as molecular dynamics, our technique serves as a bridge between computational techniques that perform mathematical modeling of the atomic forces operating on a small number of molecules and macrolevel techniques that investigate interactions between relatively large numbers of molecules in a statistical manner. By applying this model to the study of AFP−ice interactions, we have been able to duplicate key experimental results such as ice-etching patterns, ice-growth inhibition, and AFP-dependent ice-crystal morphology changes during both ice-growth inhibition and burst growth.

Two features of our model are primarily responsible for the power of this technique, the first being the move to true 3-D modeling. Previous 3-D crystal growth techniques[17,27,30−32] are in reality only two-dimensional, as they focus exclusively on a crystal *surface*, usually a flat plane, and extend this surface into the horizon by employing periodic boundary conditions. While these models can provide insights into surface properties such as nucleation events and surface roughening, our approach extends these models to investigate entire 3-D crystals, an extension that allows for the study of whole-structure phenomena such as morphology. This extension cannot be underestimated with regards to crystal growth, because surface curvature will dictate crystal growth behavior. Our technique, with its ability to model normal step growth (Figure 8A), as well as more complex localized curvatures requiring nonfunctional relationships (i.e., multiple Z spatial locations for any (X,Y) pairing in the plane) (Figure 8B), is invaluable for investigating crystal growth mechanisms both in the presence and in the absence of inhibitory molecules. Simulations of ice growth in the presence of AFPs clearly exhibit increased local curvature between bound AFPs (Figure 8B), lending support to the

(30) Xiao, R. F.; Alexander, J. I. D.; Rosenberger, F. *J. Cryst. Growth* **1990**, *100*, 313−329.
(31) Yokoyama, E. *J. Cryst. Growth* **1993**, *128*, 251−257.
(32) Jackson, K. A. *J. Cryst. Growth* **1999**, *198/199*, 1−9.

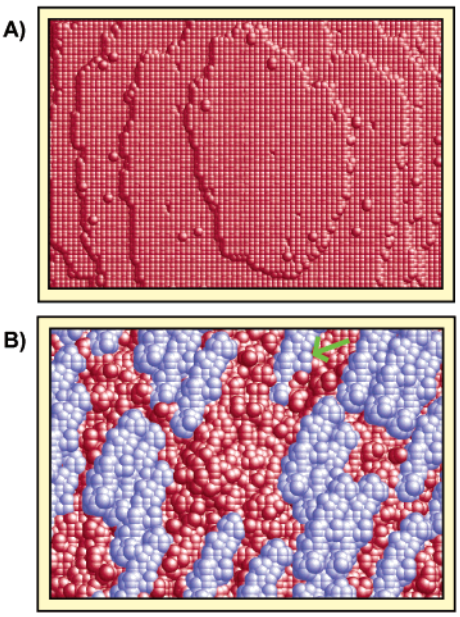

Figure 8. Prism plane growth. Figure 8A shows ice growth on the prism plane in the absence of AFPs. Step growth is clearly evident, as new nucleation events rapidly grow out to the edges of the plane. The spacing of steps relative to one another on the edges of the plane will be temperature dependent; lower temperatures will support step growth closer to the edges of previous layers, producing temperature-dependent curvature on the surface. Several single water molecules can be seen in the figure, showing the dynamic nature of ice growth as new nucleation events are spontaneously occurring. The vast majority of these nucleation events melt away. Figure 8B shows the effects of AFPs on the highly regular step growth illustrated in Figure 8A. Here, WfAFP, inhibiting ice growth at −2.0 °C, is increasing the local surface curvature by forcing ice to grow in bulges between bound AFPs. The process is highly dynamic, with ice growing and melting continuously. The AFP spacing is critical to ensuring that ice growth is contained. For example, the green arrow points to an AFP which, due to localized spacing issues, is in danger of being embedded in the ice crystal.

prevailing theory of ice-growth inhibition.[4,5] Under conditions of AFP-induced ice-growth inhibition, there is continual surface fluctuation as ice molecules melt and grow between AFPs. During burst growth, the decreased temperatures allowed increased ice curvature between AFPs, as can be seen from the highly unusual concave ice growth out of the secondary prism plane that occurs during burst growth in the presence of TmAFP (Figure 7H). Eventually curved ice fronts spill around and over bound AFPs, imbedding them within the growing ice front. A partially buried AFP can be seen in the top of Figure 8B.

The second feature of our model that contributes to its power is the addition of spatial and energetic complexity to the representations of molecules in simulations. Molecules in previous 3-D surface models are generally represented spatially by single locations in their simulation spaces.[17,27,30−32] Although this approach does allow for the statistical study of cumulative interactions between large numbers of molecules, it treats these molecules in a generic fashion and does not allow the specific spatial and electrostatic properties of these molecules to express themselves in the resulting crystal structures. In contrast, our approach represents simulation molecules as multiple simulation space locations that replicate the spatial geometry of these molecules in their stereospecific crystal-adsorption orientations. Furthermore, because molecules are spatially restricted to these adsorption orientations, the interaction energies of the resulting finite number of possible molecular orientations can be precalculated, rendering energetics information nonuniform across molecular surfaces. This increased complexity in molecular structure and energetics allows both of these properties to directly influence crystal growth behavior within our model. The 3-D structure and binding orientations of the various AFP molecules that were introduced into simulations had obvious impacts on ice-crystal growth, with respect to both ice morphology and ice-growth inhibition.

These features of our model allow for the testing of more advanced hypotheses with regards to crystal structure formation. Because simulations deal with virtual molecules, the properties of these molecules can be artificially modified to investigate their importance in determining macrolevel features of crystal structures. Questions regarding the role of molecular shape and energetics can thus be investigated directly. Several of our simulations involving AFPs and ice crystals illustrate this concept. For example, altering WfAFP and TmAFP *off* rates had little effect on antifreeze activity until the off rates were increased by an order of magnitude. These results suggest that, while ice-binding ability is a necessary prerequisite for AFP activity, the degree of antifreeze activity is *not* determined by AFP ice-binding strength. This conclusion, although contrary to prevailing views in the AFP field, does have experimental support.[23,33] It is known that slow-growing ice incorporates AFPs *into* the ice phase, in contrast to non-AFPs that are *excluded from* the ice phase. This fundamental distinction between AFPs and non-AFPs suggests that all AFPs, once correctly aligned, bind essentially irreversibly to ice, a fact that would negate binding strength as the major factor in determining the degree of AFP activity.

Attempts to understand the differences in antifreeze abilities between WfAFP and TmAFP illustrate another useful property of this computational technique: the visualization of dynamic processes containing 3-D molecules. As can be seen in Figure 7B and F, the ice surfaces covered by WfAFP and TmAFP are significantly different. Because of their respective binding orientations, WfAFP cannot bind to the basal planes of ice crystals, whereas TmAFP, given a minimal curvature on the basal plane, can. At temperatures below the antifreeze abilities of WfAFP, spicular growth occurs along the *c*-axis, directly out of that portion of the crystal to which WfAFP cannot bind (Figure 7D). TmAFP, by contrast, can bind to this plane as it adopts sufficient curvature in response to lowered temperatures, producing biconcave shaped crystals (Figure 7F) and avoiding the spontaneous burst growth that leads to the spicular morphology associated with WfAFPs. Such antifreeze protection lasts until an even lower temperature is reached, below the antifreeze abilities of TmAFP, at which point burst growth occurs at right angles to the basal plane, out of the secondary prism plane (Figure 7H). From the visual examination of numerous simulation experiments, we feel that the differences in surface coverage between these two AFPs can be understood in relation to the inherent growth patterns of hexagonal I_h ice crystals. Ice crystals that experienced *isotropic* growth (and thus equal growth in all directions) would adopt spherical morphologies; such crystals grown in the presence of two AFPs with similar shapes but different binding orientations should have essentially the same amount of crystal coverage, although at different patches on the spherical ice surface where their binding orientations are

(33) Knight, C. A.; Driggers, E.; DeVries, A. L. *Biophys. J.* **1993**, *64*, 252−259.

tangential. The differences in surface coverage between WfAFP and TmAFP, which have roughly similar rodlike structures, must therefore be a result of the anisotropic growth rates of ice crystals. This leads to the following conclusion: an AFP's activity is a result of *its binding orientation relative to the anisotropic growth of the underlying ice crystal*. At supercooled temperatures where an ice crystal is constrained from growing by the presence of AFPs, anisotropic ice growth causes each new basal step to grow rapidly *across* the basal plane toward the crystal edges. Temperature will dictate the resulting basal-plane surface curvature at the apexes of the AFP-constrained crystal. As temperatures drop, this surface curvature increases. WfAFP, with a large *c*-axis component to its binding orientation, reaches the limit of its antifreeze ability when the temperature drops sufficiently to increase the ice curvature at the crystal apexes beyond the binding ability of WfAFP; spicular growth out of these apexes ensues. In contrast, TmAFP, with its binding orientation perpendicular to the *c*-axis, has only a small *c*-axis component in its binding orientation and can thus bind readily to increased curvatures on the basal plane. In this manner, it easily advances to the apex of the ice crystal, producing biconcave crystals (Figure 7F).

While our model provides many opportunities for investigating regular crystal growth, it is not without its limitations. Because the orientation of each molecule must be fixed relative to the underlying arrangement of simulation space locations, there are difficulties in relating *on/off* rates between the various types of molecules in simulation. Molecules must not only select an interface location at which to bind to a crystal, but their 3-D structure must also be free of steric clashes with other parts of this crystal; because their orientations are fixed, this means that the number of possible binding locations available to a molecule decreases as the size of the molecule increases. One cannot simply assign molecular *on* rates on the basis of their relative concentrations in solution. Similarly, *off* rates cannot readily transfer among molecule types. The probability of an ice molecule and an AFP molecule detaching from a crystal given that they are both held to the crystal by two hydrogen bonds will not be the same; the larger AFP molecule is subject to more forces, both internal due to its higher number of constituent atoms and external due to its larger surface area, all of which will influence its dissociation probability. This *on/off* rate independence among participating molecules implies that each type of molecule must have its own independent method of establishing realistic association/dissociation probabilities. In our AFP-ice models, water *on/off* probabilities were calibrated to temperature using the established relationship between temperature and the critical radius of an ice crystal. In contrast, it must be acknowledged that our selection of AFP *on/off* rates is much less rigorous and evolved through trial and error guided by experience. We are currently exploring the use of the relationship between AFP activity level and AFP concentration to develop more rigorous approaches to AFP *on/off* rate calibrations. Other limitations to our model result from inherent properties of the Kinetic Ising model. As molecules are either associated to a crystal or not, they are presumed to disappear entirely on dissociation, certainly an unreal simplification. Another inherent limitation of Kinetic Ising models is their restricted applicability to the study of idealized crystal growth only; they cannot therefore be readily applied to the study of nonidealized crystals, including the study of crystal imperfections such as screw dislocations. Simulations involving millions of molecules are simply not computationally feasible without absolute uniformity in the resulting structures. Some further complexity can be added to our model by adopting more complex association/dissociation rates for the participating molecules, perhaps ones that consider such environmental factors as local temperature fluctuations, but here again the amount of complexity added will quickly be curtailed by computing power.

In conclusion, our computational model, combining the statistical approach of macrolevel techniques with some of the detailed energetics calculations of molecular mechanics techniques, provides new opportunities to explore the formation of dynamic structures composed of a variety of complex molecules. Our initial application of this model to the study of AFPs has been effective at duplicating key experimental evidence with regards to AFP−ice interactions and has provided insight into the mechanisms of AFP activity. It is hoped that this model will be able to provide further insight into such questions as the nature of the relationship between AFP concentration and activity, the necessity of irreversible binding for antifreeze activity, and, through the creation of a series of artificial AFPs with increasing *c*-axis components in their binding orientations, the exact relationship between AFP binding orientation and activity. This model could readily be adapted to study other crystal and crystal inhibitor systems (e.g., the inhibition of calcium carbonate crystals in the pancreas by lithostathine protein) or to other noncrystal systems that exhibit regularity in the structuring of their component molecules, such as those associated with the new nanotechnologies.

Acknowledgment. This work is supported by Canadian Institutes of Health Research and Natural Sciences and Engineering Research Council of Canada. We thank Dr. Peter Davies for insightful discussion and encouragement. We would also like to acknowledge the dedication of an anonymous and most knowledgeable referee. Z.J. holds a Canada Research Chair in Structural Biology.

JA0267932